Journal of Colloid and Interface Science 554 (2019) 239–249

Contents lists available at ScienceDirect

Journal of Colloid and Interface Science

journal homepage: www.elsevier.com/locate/jcis

Regular Article

Gold nanoparticles modified hollow carbon system for dual-responsive release and chemo-photothermal synergistic therapy of tumor

Qinfu Zhao, Yang Yang, Huili Wang, Wei Lei, Yixuan Liu, Siling Wang *

Department of Pharmaceutics, School of Pharmacy, Shenyang Pharmaceutical University, 103 Wenhua Road, Shenyang, Liaoning Province 110016, PR China

GRAPHICAL ABSTRACT

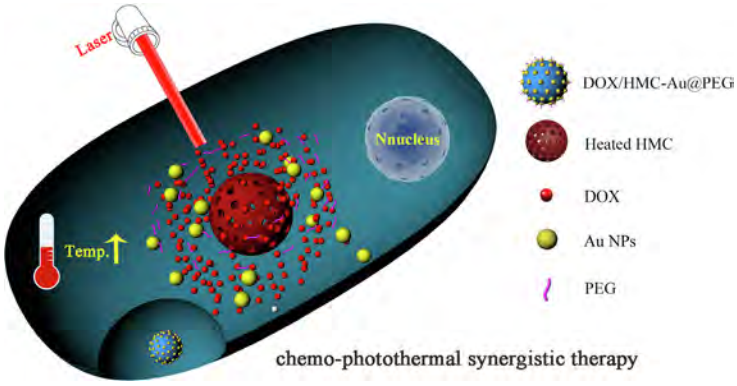

ARTICLE INFO

Article history:
Received 28 April 2019
Revised 1 July 2019
Accepted 3 July 2019
Available online 3 July 2019

Keywords:
Hollow mesoporous carbon
Gold nanoparticles
Thermochemotherapy
Au—S bonds
Doxorubicin

ABSTRACT

Thermochemotherapy has shown a synergistic anti-cancer efficiency and can enhance the therapeutic effect of simple chemotherapy. The photothermal conversion characteristics of carriers are vital in thermo-chemotherapy. Therefore, hollow mesoporous carbon (HMC) with excellent heating efficiency and a large specific surface area was used to ensure the high loading capacity. Next, approximately 4 nm spherical gold nanoparticles (NPs) were employed as gatekeepers of the tunnels of HMC by Au-S bonds, which have the same size as HMC mesopores. Additionally, the gold NPs could avoid the premature release of the drug and enhance the photothermal properties of the delivery system. The surface of the carriers was modified with polyethylene glycol (PEG) to increase the biocompatibility and dispersity of doxorubicin (DOX) loaded DOX/HMC-Au@PEG. DOX release was markedly accelerated in the presence of glutathione (GSH) and near-infrared (NIR), indicating that the system had redox and NIR dual-triggered drug release characteristics. Cytotoxicity experiments proved that combined therapy induced the highest cell killing level. Additionally, the combination index (CI) of DOX/HMC-Au@PEG was 0.452, indicating the synergistic effect of chemotherapy and photo-thermal therapy (PTT). *In vivo* antitumor experiments were also carried out and showed the same trend. In general, the results of this study indicated that DOX/HMC-Au@PEG has great potential in dual-triggered drug delivery and thermochemotherapy.

1. Introduction

Presently, tumors pose a serious threat to human health but there are many ways to treat tumors, the most common of which

* Corresponding author.
E-mail address: silingwang@syphu.edu.cn (S. Wang).

https://doi.org/10.1016/j.jcis.2019.07.005
0021-9797/

are surgery, radiation and chemotherapy [1]. However, these treatments have many side effects and may hurt the human body.

As a new and noninvasive method to treat tumor, photothermal therapy (PTT) has gained increasing attention [2–5]. In external light irradiation, the near-infrared (NIR) adsorbing carriers convert light energy into heat to kill tumor cells. NIR (800–1200 nm) light is the transmission window of body tissues; compared with other wave bands, NIR light has the highest transmittance in the body tissues and the least damage to human body [6]. Furthermore, the treatment time of PTT is short, and the treatment effect is obvious. Because individual chemotherapy is hard to meet therapeutic needs, the combination of PTT and chemotherapy has become a promising alternative for the treatment of tumors [7–9]. Chemotherapy and hyperthermia reagents are delivered to tumor sites together through a nano-system. With the help of NIR laser irradiation, the hyperthermia reagent could generate heat in the tumor cells, making the chemotherapeutics more effective and kill cancer cells easily [10]. The chemo-photothermal synergistic therapy can reduce the side effects and provide new possibilities for cancer treatment.

With the development of PTT, four generations of material systems have been developed [11], including (1) precious metal nanoparticles: Au, Ag and Pt [12,13]; (2) carbon materials: graphene, carbon nanorods [14–16]; (3) metals and non-metallic compounds: CuS, ZnS [17]; (4) organic dye: indocyanine green and prussian blue [18]. In recent years, the studies on carbon materials are quite active. As a representative carbon material, hollow mesoporous carbon (HMC) nanoparticles have many unique advantages. HMC has the characteristics of large specific surface area, high loading capacity and easily functionalized surface. Meanwhile, compared with other mesoporous carbon materials, HMC possesses lighter density and higher heat conversion efficiency due to the distinctive hollow structure [19].

The photothermal conversion characteristics of delivery systems are vital in thermo-chemotherapy. To further enhance the effect of hyperthermia, gold nanoparticles (NPs) with good photothermal properties have attracted wide attention. Gold NPs materials have a wide range of important applications in the field of biomedicine due to its biocompatibility and unique physical and chemical properties [20]. Because of the surface plasmon resonance (SPR), in the visible to NIR region, the absorption peak of gold NPs is adjustable [21]. Gold NPs themselves have the characteristic of heating up, and their shapes and particle sizes can be controlled; thus they are suitable as the capping to hinder the drugs within the mesopores. After the gold NPs were modified on the surface of HMC, the photothermal conversion efficiency was enhanced with the cooperation of HMC and gold NPs, and the two materials could exert a synergistic effect in PTT.

In this work, HMC with excellent photothermal conversion efficiency was designed, and gold NPs was used as the capping, for the first time, to avoid premature release of drugs and increase the photothermal properties of HMC. The aperture of HMC and diameter of gold NPs are both approximately 4 nm, and the openings of HMC were decorated by the spherical gold NPs through Au-S bonds as shown in Scheme 1 [22–24]. The Au—S bonds and disulfide bonds have the same property, so the Au—S bonds will be disconnected under the high concentration of glutathione (GSH) [25]. The antitumor drug doxorubicin (DOX) was loaded into the cavity of HMC, and the modified PEG on the surface of HMC-Au could enhance the biocompatibility and dispersity of HMC-Au@PEG [26]. When DOX/HMC-Au@PEG was taken up by cells, the Au-S bonds were cleaved with GSH, and DOX was released. Simultaneously, under NIR irradiation, the HMC and gold NPs will convert NIR light into cytotoxic heat, accelerating the release of the loaded DOX. Finally, DOX and PTT could produce a synergistic effect. The drug delivery system was characterized by various methods. *In vitro* photothermal heating effects and thermal stability of carboxylated HMC (HMC-COOH) and HMC–Au@PEG as well as the redox and NIR dual-triggered drug release effect of DOX/HMC-Au@PEG were studied. Additionally, the *in vitro* and *in vivo* combined antitumor therapies were evaluated to demonstrate synergistic chemo-photothermal therapy.

2. Materials and experimental conditions

2.1. Reagents and materials

1-(3-dimethylaminopropyl)-3-ethylcarbodiimide hydrochloride, 3-mercaptopropionic acid (98%), sodium borohydride ($NaBH_4$, 98%), chloroauric acid, 2-(7-Azabenzotriazol-1-yl)-N,N,N',N'-tetra

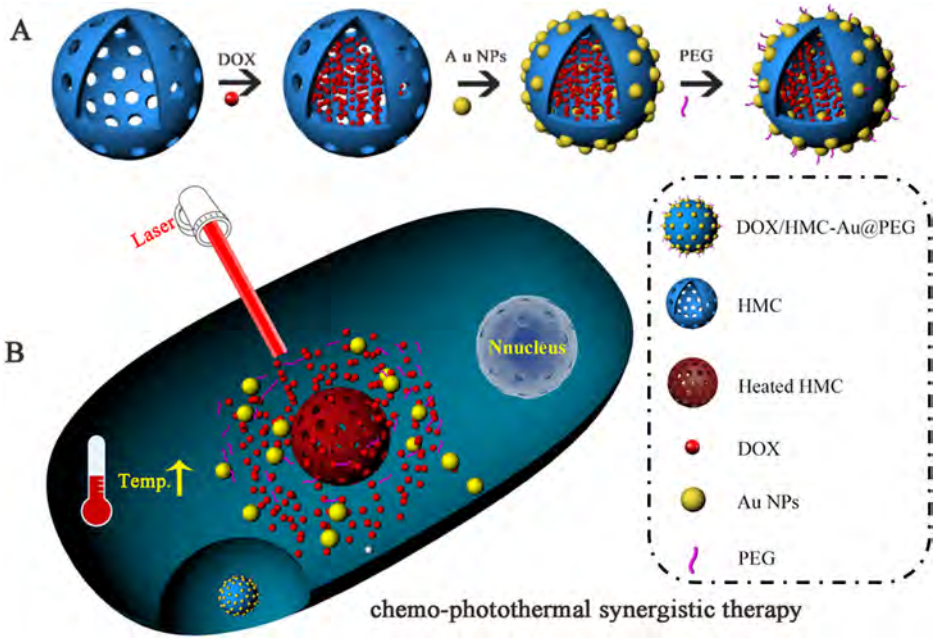

Scheme 1. (A) Drug loading procedure of DOX/HMC-Au@PEG. (B) Combined photothermal therapy and chemotherapy for tumors.

methyluronium hexafluorophosphate (HATU, 99%), thiolated poly (ethylene glycol) monooxygen ether (PEG-SH, Mw = 2000), trisodium citrate (99%) and glutathione (GSH, 98%) were purchased from Aladdin (Shanghai, China). Doxorubicin hydrochloride (DOX, 98%), Fetal bovine serum (FBS), Roswell Park Memorial Institute (RPMI)-1640 and fluorescent Hoechst 33,258 were all attained from Dalian Meilun Biotechnology Co., Ltd. (Dalian, China). Deionized water was prepared by Millipore (Bedford, MA, USA). All other reagents and solvents of analytical grade were used as received unless otherwise mentioned.

2.2. Preparation of DOX/HMC–Au@PEG

2.2.1. Preparation of HMC and HMC-SH

The carrier of HMC was prepared according to our published method [27]. HMC-COOH was prepared as described previously [19] and then was further modified to obtain HMC-NH_2. Briefly, 200 mg of HMC-COOH was added to 100 mL of ethylenediamine, and then 20 mg of HATU was added into the solution. After stirring for 12 h, the product HMC-NH_2 was collected by centrifugation by 10 000 g for 5 min. Finally, the mercapto group was attached to the surface of HMC by an amidation reaction. Thereafter, 60 mg mercaptopropionic acid was dispersed in 20 mL water, 35 mg EDC and 25 mg NHS were added into the solution to activate carboxyl, and then the activated mercaptopropionic acid was added into the HMC-NH_2 suspension, followed by continued stirring of the suspension for 1 day. The obtained product was named HMC-SH.

2.2.2. Preparation of gold NPs

The preparation of gold nanoparticles refers to a classical method with some modifications [28]. Equivalent concentrations of chloroauric acid (0.25 mM) and sodium citrate were mixed evenly. Next, 0.1 M $NaBH_4$ was poured into the above solution. After further stirring for 4 h, the prepared gold NPs were stored at 4 °C.

2.2.3. Preparation of DOX/HMC-Au@PEG

HMC-SH (10 mg) was dispersed uniformly in pH 7.4 PBS, 5 mL DOX solution at 1.5 mg/mL was added into the above solution, followed by continued stirring for 12 h in the dark. The product was denoted as DOX/HMC-SH. To decorate gold NPs on the surface of HMC, 50 mL of gold NPs was dispersed in the DOX/HMC-SH suspension and continued to stir for another 12 h. The resulted product obtained was named as DOX/HMC-Au. In order to enhance the biocompatibility of the system, PEG was modified on the surface of the carrier. 400 μL 5 mM of PEG-SH was added to above solution, and the obtained product was DOX/HMC-Au@PEG. The product was centrifuged by 10 000 g for 5 min, the supernatant was collected and volumetrically adjusted with a volumetric flask. Then the absorbance was measured by UV–Vis spectrophotometry to evaluate the drug loading efficiency of DOX in the carrier. The total amount of DOX loaded in the DOX/HMC-Au@PEG was calculated by subtracting the unabsorbed DOX in the supernatant from the initial amount of DOX added. Moreover, the synthesis of the unload carrier system of HMC-Au@PEG was the same as above procedure.

2.3. NIR-triggered heating effect studies

The HMC-COOH and HMC-Au@PEG suspensions were irradiated with an 808 nm NIR laser equipment to verify the photothermal conversion efficiency. Next, 0.2 mL of different concentrations of the carrier suspensions were filled into 0.5 mL EP tube, and followed by irradiation at 2 W/cm^2 for 3 min. Apart from this, the NIR laser equipment was set to different powers to irradiate 50 μg/mL of carrier suspension.

2.4. In vitro stimuli-responsive and NIR-triggered release of DOX

The pH 5.0 PBS and pH 7.4 PBS were used to mimic tumor microenvironment and body fluid. And DOX/HMC-Au@PEG was dispersed in different media solutions containing different concentrations of GSH. Next, the samples were placed in a constant-temperature shaking table for 1 d at 37 °C. After a certain period of time, the samples were taken out, centrifuged by 8 000 g for 5 min, and the absorbance was measured by UV–Vis spectrophotometer at 480 nm. Moreover, the NIR-triggered release of DOX was similar to the above method. The only difference is that the suspension was irradiated at 2 W/cm^2 for 3 min using an 808 nm NIR laser equipment.

2.5. NIR-induced cellular photothermal effect studies

4T1 cells were seeded into 6-well plates at a density of 2×10^5 -cells/well. After culturing, the cell culture fluid was replaced with different concentrations of HMC-COOH and HMC-Au@PEG suspensions (10, 25, 50 and 100 μg/mL). The cells were incubated with the carriers for 2 h, and then 500 μL of trypsin was added to each well to digest cells, followed by continued to culture for 3 min. Thereafter, the digested cells were dispersed in 400 μL of 1640 medium and centrifuged. Next, the centrifuged cells were re-dispersed in 200 μL of PBS and irradiated at 2 W/cm^2 for 150 s.

2.6. Characterizations

Transmission electron microscopy (TEM) (Tecnai G^2F30; FEI; Eindhoven, Netherlands) was used to observe the basic morphology of the carrier. Elemental analysis was measured using an ESCALAB 250 spectrometer (Thermo Fisher Scientific, USA) with an Al-Kα X-ray source. The size distribution was measured using the Particle Size Analyzer Nicomp 380 (Particle Sizing Systems, USA). The FT-IR spectrometer (Bruker IFS 55, Faellanden, Switzerland) was used to measure a Fourier transform infrared (FT-IR) spectrophotometric spectrum. A surface area adsorption analyzer (V-Sorb 2800P, Gold APP Instrument Corporation, Beijing, China) was used to characterize the surface area and pore distribution of the carriers.

2.7. Cell uptake

The 4T1 cell uptake of the carriers was characterized by confocal laser scanning microscopy (CLSM). The cells were counted and seeded into 24-well plates with a density of 5×10^4 cells/well. After culturing for 1 d, the cell medium was replaced with the suspension of HMC-Au@PEG, DOX/HMC-Au@PEG, and free DOX (equal to 5 μg/mL DOX). After continued culture for 2 h, the cell medium was poured out and rinsed with PBS for three times. For NIR irradiation group, DOX/HMC-Au@PEG was irradiated with an 808 nm laser at 2 W/cm^2 for 5 min and was further incubated for another 1 h. The wells containing DOX/HMC-Au@PEG absence of NIR laser after washing were used as a negative control. Next, 4% formaldehyde was added to each well, and Hoechst 33,258 was added to stain the nuclei, and the cell uptake was observed in a Leica DM-6000 CS microscope (Leica Instruments, Inc., Wet-zlar, Germany).

2.8. In vitro NIR-induced cytotoxicity test

The MTT (3-(4,5-dimethylthiazol-2-yl)-2,5-diphenyltetrazolium bromide) assay was used to evaluate the NIR-induced photothermal cytotoxicity. 4 T1 cells were seeded in 96-well plates at a density of 2×10^4 cells/well. After 1 d the original medium was discarded and DOX samples with different concentrations (0.01, 0.1, 1.0, 5.0 and 10 μg/mL) were added into the

corresponding well. After cultivating for 1 d, 50 μL MTT solution was added, followed by continued culture for 4 h. Thereafter, we added 150 μL DMSO to each well to dissolve the formazan crystals. Finally, the absorbance of each well at 570 nm was recorded with a microplate. Regarding photothermal treatment, the only difference was that the cell suspensions were irradiated for 3 min during the cell culture, and the illumination power was set to 2 W/cm^2. The combination index (CI) was calculated according to the equation: $CI = [IC_{50\ (combined\ chemotherapy)}/IC_{50\ (chemotherapy)}] + [IC_{50\ (combined\ PTT)}/IC_{50\ (PTT)}]$. The value of CI < 1 indicates synergism, CI > 1 means antagonism, and CI = 1 shows additive effects.

2.9. In vivo combination therapy, biodistribution study and histological examination

Female KM mice were provided by the Shenyang Pharmaceutical University animal center. All experimental procedures comply with the guidelines of the Animal Protection and Ethics Committee of Shenyang Pharmaceutical University. The mice were subcutaneously administered with 2×10^6 4T1 cells under the armpit of the right forelimb. When the tumor volume was increased to approximately 100 mm^3 (the tumor volume = width^2 × length/2 [29]), the tumor-bearing mice were randomly divided into five groups—saline, free DOX, DOX/HMC-Au@PEG, HMC-Au@PEG with NIR irradiation and DOX/HMC-Au@PEG with NIR irradiation. The mice were injected every other day for 3 times. The drug concentration of each group was identical to the DOX concentration of 10 mg/kg. For the NIR treatment groups, after intravenous injection in mice for 2 h, the tumor site was irradiated at 1 W/cm^2 for 180 s. The body weight and tumor volume of the mice were measured every other day. On the 17th day, the mice were sacrificed and the tumor was removed and weighed. Additionally, as the tumor volume increased to 200 mm^3, the tumor-bearing mice were randomly divided into 3 groups—free DOX, DOX/HMC-Au@PEG without NIR and DOX/HMC-Au@PEG with NIR. The mice were injected with 200 μL of the corresponding suspensions at a concentration equivalent to 10 mg/kg of DOX. Next, the mice were sacrificed at 2 h, 6 h, and 12 h, and then the tumor and other major organs, including the heart, liver, spleen, lung and kidney, were removed. The distribution of DOX in each organ was observed using Carestream Molecular Imaging software. The excitation wavelength was set to 470 nm, and the emission wavelength was set to 535 nm [30]. Moreover, H&E staining further verified the degree of damage to different organs.

3. Results and discussion

3.1. Preparation and characterization of HMC-Au@PEG

The synthetic route of HMC-Au@PEG is shown in Scheme 1. Through the amidation reaction, -SH was first decorated on the surface of HMC. Next, the Au NPs, as gatekeepers, were decorated on the tunnels of the carrier through Au-S bonds. Finally, PEG was decorated on the surface to enhance the biocompatibility of the whole system. The TEM of the prepared HMC is shown in Fig. 1 (A); a uniform hollow and channel structure could be clearly shown in the figure. Additionally, the average diameter of HMC was (149 ± 10) nm (n = 30), and the mesoporous layer thickness was (31.2 ± 4.4) nm (n = 30). Spherical gold NPs with an average diameter of (3.9 ± 1.1) nm (n = 100) were observed in Fig. 1(B). The HRTEM images of HMC-Au@PEG are shown in Fig. 1(C) and (D), many gold NPs could be markedly observed on the surface of HMC. The gold NPs with a similar size to the carrier mesopores were modified on the openings of HMC. Therefore, gold NPs could block the tunnel to prevent the drug from being released before it reaches the designated site. In addition to this finding, AFM was further applied to characterize the gold NPs as shown in Fig. 1(E) to (G). As shown in Fig. 1F, the average height of gold NPs was close to 4 nm, which was very close to the diameter of gold NPs observed by TEM.

Additionally, the characterizations of the system are shown in Fig. 2. Fig. 2(A) shows the changes in the Zeta potential in each grafting process. The Zeta potentials of HMC-COOH, HMC-NH_2, HMC-Au and HMC-Au@PEG were −27.7 mV, 10.7 mV, −39.1 mV and −8.1 mV, respectively. The results showed that the positively charged amino group of HMC-NH_2 was grafted on the outer layer of HMC-COOH, and the grafting of PEG could reduce the negative charge of HMC-Au@PEG. Additionally, the particle size of HMC-COOH, HMC-NH_2, HMC-Au and HMC-Au@PEG are shown in Table S1, with continuous modification of the functional groups, the particle sizes of the nanoparticles gradually increased. And the polydispersity index (PDI) of HMC-Au@PEG was smaller than that of the other nanoparticles, indicating good dispersity after the grafting of PEG. The FT-IR spectra are shown in Fig. 2(B), and the HMC was used as a blank control. Regarding HMC-NH_2, the appearance of a new absorption peak at 1520 cm^{-1} was the characteristic peak of -NH_2. After PEG was modified on the surface of the carrier, the new characteristic peaks appeared at 2952 cm^{-1} and 2922 cm^{-1}. The series of processes proved the synthesis of HMC-Au@PEG. The graft degree of PEG in HMC-Au@PEG was verified by the standard Ellman's assay based on the quantification of mercapto groups in PEG-SH [31]. And the graft amount of PEG-SH in HMC-Au@PEG was calculated to be 14.2%. Additionally, the visible and NIR spectra were used to further characterize the carrier as shown in Fig. 2(C). Gold NPs, HMC-Au and HMC-Au@PEG all showed the absorption peak at 510 nm, indicating that the Au NPs have been deposited onto the surface of the carrier. Furthermore, the X-ray photoelectron spectroscopy (XPS) were used to characterize HMC-Au@PEG, and the specific data are shown in Table 1. Compared to HMC, the appearance of a new peak of Au 4f proved the preparation of HMC-Au in Fig. 2(D). In the HMC, the proportion of C was 74.71% and that of O was 23.42%. For HMC-Au, the elemental proportion of Au was increased to 3.84%. Furthermore, due to the large amount of methylene in PEG, the proportion of C in the HMC-Au@PEG was increased from 61.75% to 75.11%, and the proportion of Au and S were reduced to 0.71% and 1.03%, respectively. These results indicated the successful preparation of HMC-Au@PEG.

The pore size distributions and isotherms were characterized by N_2 analysis as shown in Fig. 2(E) and (F). Additionally, the specific value of S_{BET}, pore diameter distribution (D_P) and pore volume (V_t) are displaced in Table S2. From HMC to HMC-SH, the S_{BET}, D_P and V_t had a tendency to gradually decrease. The D_P of HMC-SH was 3.7 nm, indicating that internal mesopores of HMC still existed after the multiple-step modification. As shown in Fig. S1, HMC-Au indicated poor dispersibility in the physiological saline condition and precipitated rapidly after dispersion for 2 h. However, the stability of HMC-Au@PEG markedly increased after the modification of PEG. HMC-Au@PEG nanoparticles can remain stable for up to 6 h under physiological PBS. Moreover, the bovine serum albumin (BSA) adsorption experiment (Table S3) showed that the adsorption of BSA for HMC-Au@PEG markedly decreased from 15.39% (for HMC-Au) to 1.89% after the modification of PEG. The results further demonstrated that the modification of PEG can reduce the adsorption capacity and enhance the biocompatibility of the carrier.

3.2. NIR-triggered heating effect of HMC-Au@PEG

An 808 nm NIR irradiation laser was used to illuminate the suspension to research the *in vitro* NIR-triggered heating effect. First, HMC-COOH and HMC-Au@PEG were both dispersed in distilled

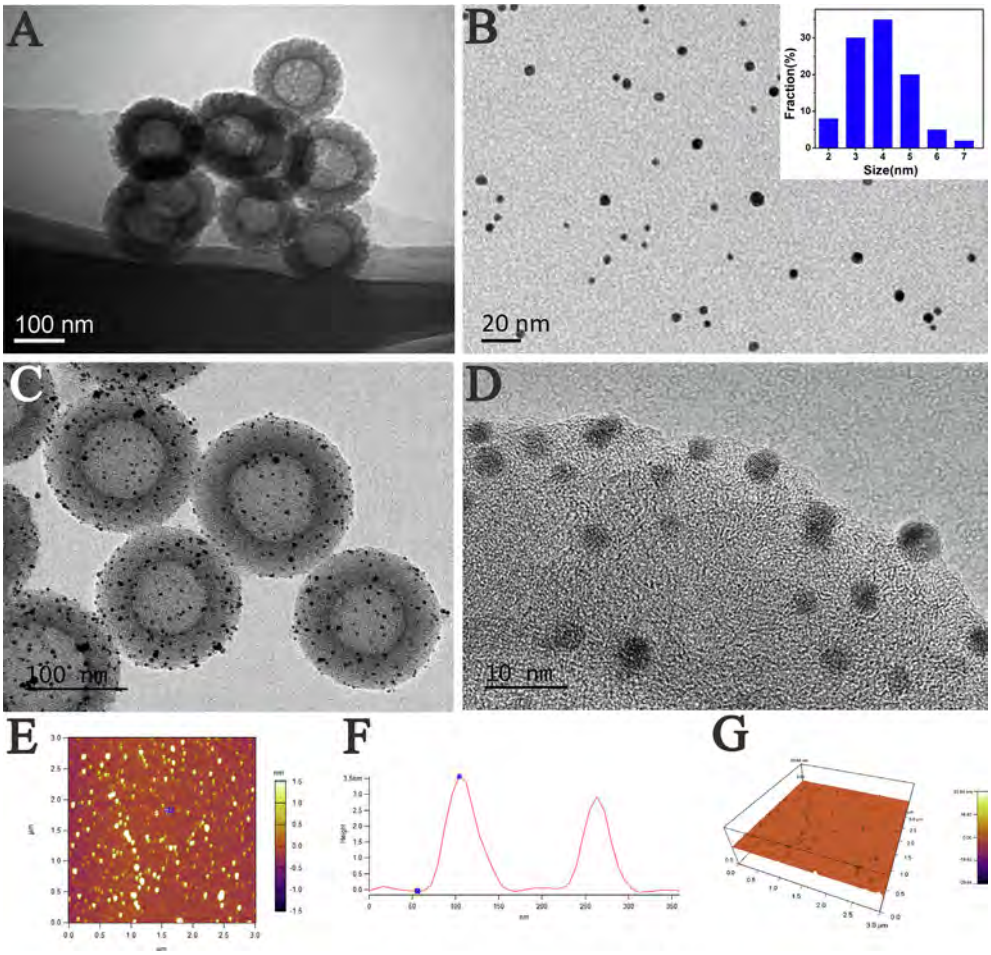

Fig. 1. TEM images of (A) HMC, (B) gold NPs, (C) and (D) HMC-Au@PEG. AFM image (D), the height (E) and dimensional image (F) of gold NPs.

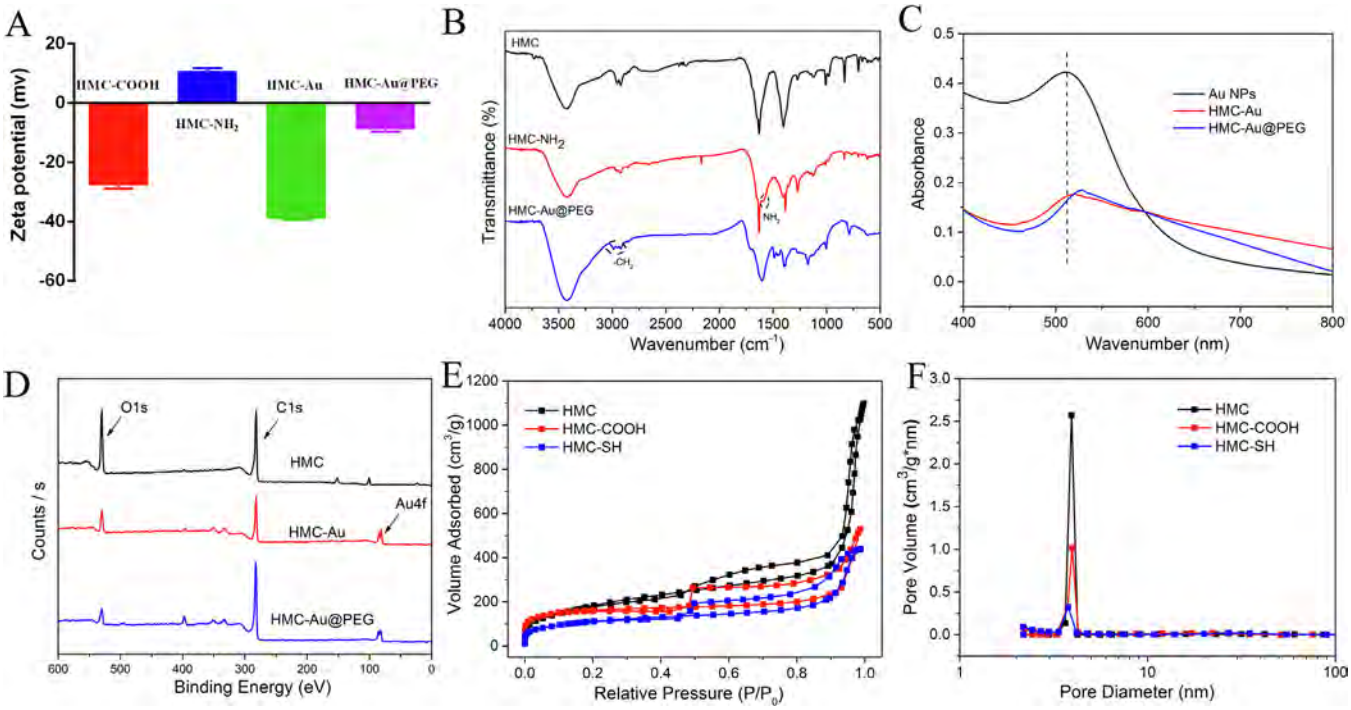

Fig. 2. (A) Zeta potential of HMC-COOH, HMC-NH_2, HMC-Au and HMC-Au@PEG in PBS at pH 7.4 (n = 3). (B) FTIR spectra of HMC, HMC-NH_2 and HMC-Au@PEG. (C) Vis-NIR spectra of gold NPs, HMC-Au and HMC-Au@PEG. (D) X-ray photoelectron spectroscopy of HMC, HMC-Au and HMC-Au@PEG. (E) N_2 adsorption-desorption isotherms and (F) pore size distributions of HMC, HMC-COOH and HMC-SH.

Table 1
Elemental analysis of HMC, HMC-Au and HMC-Au@PEG (Atomic percentage).

Samples	C (%)	O (%)	Au (%)	S (%)
HMC	74.71	23.42	–	–
HMC-Au	61.75	25.75	3.84	2.19
HMC-Au@PEG	75.11	15.94	0.71	1.03

water to prepare the suspension at the concentration of 100 μg/mL, and the thermal images are shown in Fig. S2. Under NIR irradiation for 3 min at 2 W/cm^2, the distilled water did not heat up and was used as a control. However, the temperature of HMC-COOH could reach 65 °C, and the temperature of HMC-Au@PEG could even reach 78 °C. The results indicated that the decorated gold NPs and HMC could play a synergistic effect to raise the temperature. Additionally, the elevated temperature of the HMC-Au@PEG suspension was much higher than that of mesoporous carbon [32] and gold modified mesoporous silica nanoparticles [28] in the reported literatures under the same condition. The photothermal results of gold NPs with different powers are shown in Fig. 3(A). When different powers were used to irradiate the suspensions, the temperature of gold NPs was also gradually increased with the increase in irradiation power. Fig. 3(B) shows the thermal images of gold NPs at different time points. Under the irradiation of 3 W/cm^2 for 180 s, the temperature of the gold NP suspension could close to 44 °C. The results proved that the gold NPs themselves had the characteristics of heat conversion capacity. The heating trend of HMC-COOH and HMC-Au@PEG were similar to that of gold NPs, and the temperature elevated curves are shown in Fig. 3(C) and (D). As the irradiation power increased, the temperature of the suspensions also gradually improved. Regarding the HMC-Au@PEG suspension, under the irradiation for 3 min at a power of 3 W/cm^2, the suspension temperature could even reach 93 °C; however, the suspension of HMC-COOH could only reach 72 °C. And the results remained the same compared with other powers, proving that HMC-Au@PEG had an obvious heat-production capacity.

Considering the results of the photothermal study under different powers of irradiation, the heating effects of different concentration suspensions were studied, and 2 W/cm^2 was a good choice. The concentration ranges of HMC-COOH and HMC-Au@PEG suspensions were both from 5 to 100 μg/mL. The heat-conversion efficiency was positively correlated with the concentration of carriers as shown in Fig. 3(E) and (F). Compared with bare HMC-COOH, the temperature of HMC-Au@PEG was much higher

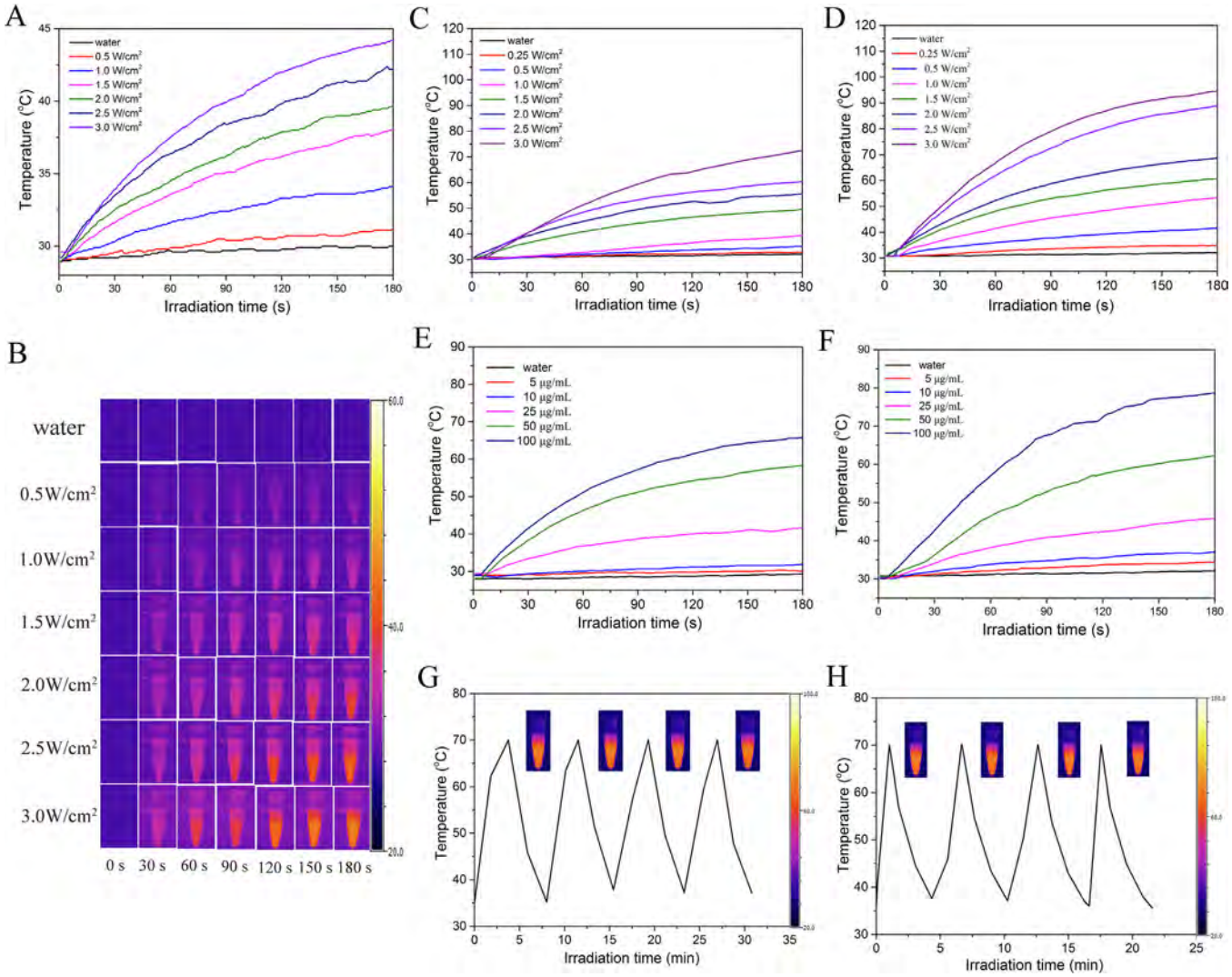

Fig. 3. (A) NIR-induced heat generation of gold NPs (50 μg/mL). (B) Thermal images of gold NPs. NIR-induced heat generation of (C) HMC-COOH and (D) HMC-Au@PEG suspension with the concentration of 100 μg/mL at different laser powers. NIR-induced heat generation of different concentrations of (E) HMC-COOH and (F) HMC-Au@PEG suspension irradiated at a power density of 2 W/cm^2. Repeated heating curve of the (G) HMC-COOH and (H) HMC-Au@PEG at a power density of 2 W/cm^2.

at the same concentration, indicating that the gold NPs and HMC-COOH had a synergistic photothermal conversion capacity. Moreover, the heating characteristics of HMC-SH under NIR irradiation are shown in Fig. S3. HMC-SH had the same photothermal efficiency as HMC-COOH, and it also had concentration-dependent and power-dependent heating characteristics. This is due to the fact that the heating effect of HMC-SH and HMC-COOH are both ascribed to the thermal conversion efficiency of HMC material. Additionally, Fig. 3(G) and (H) showed the photothermal stability of HMC-COOH and HMC-Au@PEG. After continuous NIR laser irradiation and cooling process four times, the both carriers remained in good thermal stability.

3.3. In vitro redox-responsive and NIR-triggered drug release

The loading amount of drug DOX in DOX/HMC-Au@PEG reached 40.6%, which was much higher than that of the mesoporous carbon carrier and other mesoporous carriers [10,28]. The relatively high loading capacity of HMC-Au@PEG was due to the high specific surface area, mesoporous structure, low density of carbon material, particularly, the hollow cavity of HMC [19]. It is well known that the pH in blood and normal tissues is close to 7.4, while the pH in the endosomes and lysosomes are both close to 5.0. The DOX/HMC-Au@PEG was dispersed in four release media to mimic the internal environment. In pH 7.4 PBS without GSH, the release of DOX was only 10.3% within 48 h; however, while in pH 7.4 PBS containing 10 mM GSH, the cumulative release increased nearly 2 times and became 19.5% within the same time. This is due to the Au—S bands being disconnected, and HMC-Au@PEG being reduced to HMC-SH in the presence of a high concentration of GSH, and the gold NPs could detach from the opening of HMC, leading to the accelerated release of DOX. The result showed the same tendency in pH 5.0 PBS. The cumulative release increased from 14.8% to 33.4% with the concentration of GSH increased from 0 to 10 mM GSH. These results indicated that DOX/HMC-Au@PEG had the characteristic of redox-responsive drug delivery. Additionally, the release amount in pH 5.0 PBS was much higher than that in pH 7.4 PBS.

Drug release results showed that the gold NPs could avoid the premature release of DOX, and the system had potential in thermochemotherapy. Moreover, NIR laser irradiation could have an impact on the cumulative release of DOX. To explore this effect, an 808 nm NIR irradiation laser was used. The operation was similar to that without NIR irradiation. The only difference was that the suspension was irradiated for 1, 3, 6 and 8 h at 2 W/cm^2 for 3 min, respectively. The NIR-triggered release results are shown in Fig. 4(B) and (C). In pH 7.4 PBS, the cumulative release was increased step-by-step under NIR irradiation, and the release rate of DOX was twice as high as that for without laser irradiation condition within 12 h. The result was the same as above in pH 5.0 PBS. In addition, the step-wise release profiles under the NIR irradiation have statistically significant compared with that without the NIR irradiation. Fig. 4(D) and (E) show the thermal images in pH 7.4 and pH 5.0 PBS. Under the irradiation of 2 W/cm^2 for 3 min, the temperature was markedly increased and could accelerate the drug release. Additionally, the same concentration of the HMC-COOH and HMC-Au suspension was incubated with 10 mM GSH, and then the mixtures were shaken in the shaking table. After 12 h, the supernatants of the two suspensions were collected by centrifugation and irradiated at 2 W/cm^2 for 180 s. The results further proved that gold NPs were modified on the surface of HMC, and the system had the characteristic of redox-responsiveness.

3.4. NIR-induced cellular test, cellular uptake and in vitro cytotoxicity studies

The results of the NIR-induced cellular photothermal effect are shown in Fig. 5(A) and (B). After culturing 4T1 cells with different concentrations of carriers, the cell suspensions were irradiated at 2 W/cm^2 for 150 s. Compared with the HMC-COOH suspension, the HMC-Au@PEG suspension warmed faster. And the heating rate also gradually increased with the increased concentration of

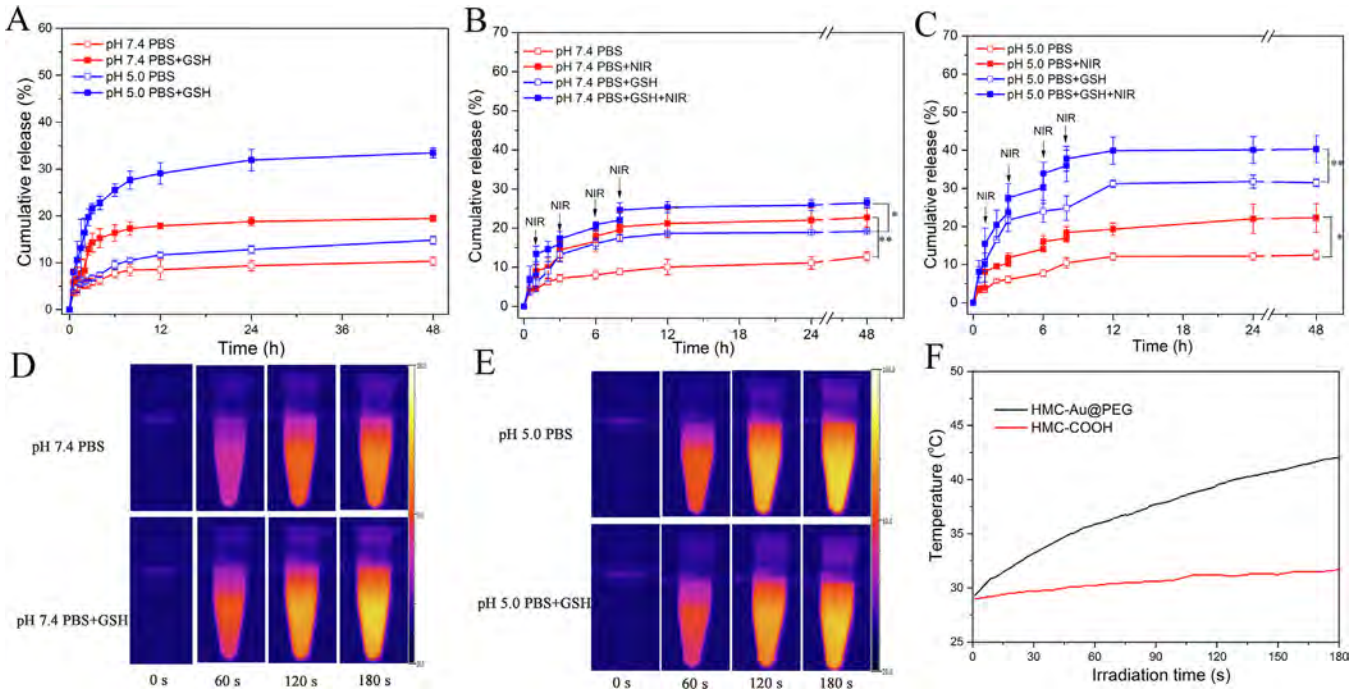

Fig. 4. (A) Release profiles of DOX from DOX/HMC–Au@PEG at different pH values with or without 10 mM GSH (n = 3). Release profiles of DOX/HMC–Au@PEG with or without NIR irradiation for 2 min at the power density of 2 W/cm^2 in (B) pH 7.4 PBS and (C) pH 5.0 PBS (* means $p < 0.05$, ** means $p < 0.01$, n = 3) (D) Thermal images of DOX/HMC–Au@PEG at pH 7.4 PBS and (E) at pH 5.0 PBS. (F) The photothermal effects of HMC-COOH and HMC–Au@PEG supernatant solution.

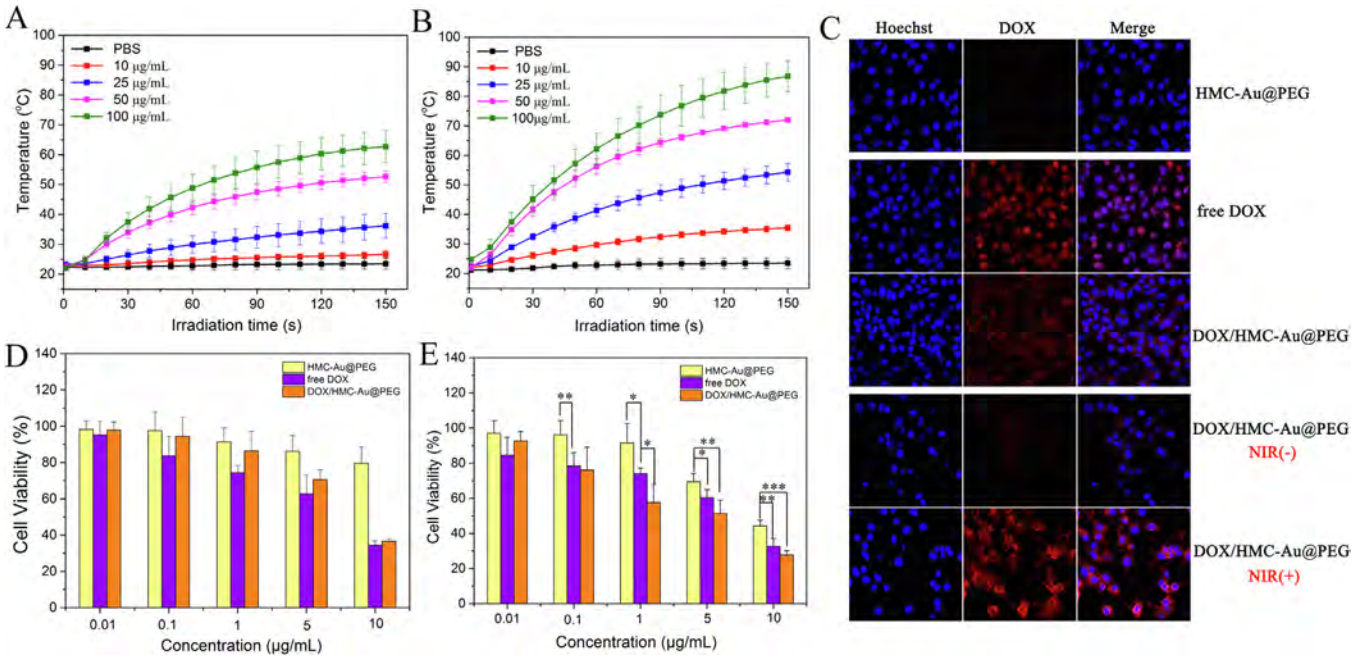

Fig. 5. NIR-induced cellular photothermal effect of 4T1 cells incubated with different concentrations of (A) HMC-COOH and (B) HMC-Au@PEG under the NIR irradiation at 2 W/cm^2 for 3 min (n = 3) (C) *In vitro* cellular uptake of HMC-Au@PEG, free DOX and DOX/HMC-Au@PEG with or without NIR irradiation at the excitation wavelengths of 408 nm and 561 nm. Cell viability of 4T1 cells toward free DOX, blank HMC-Au@PEG and DOX/HMC-Au@PEG incubation for 24 h (D) without NIR laser irradiation or (E) with NIR laser irradiation at a 2 W/cm^2 irradiation for 3 min (n = 5).

HMC-Au@PEG. As we all know that when the temperature is higher than 42 °C for several minutes, the tumor cells would be killed [33]. Additionally, the temperature of HMC-Au@PEG could be higher than 42 °C within 1 min of NIR irradiation at the concentration of 50 μg/mL, proving that the tumor cells could be killed. Next, the effect of the HMC-Au@PEG suspension was better than that of the HMC-COOH suspension. The results further proved that the HMC-Au@PEG suspension had high heat conversion efficiency and would play a good role in future tumor treatment. Additionally, CLSM was applied to study the uptake of DOX in HMC-Au@PEG by 4T1 cells as shown in Fig. 5(C). For HMC-Au@PEG, only blue fluorescence stained by Hoechst appeared, and gold NPs itself would not fluoresce at the excitation wavelengths of 408 nm and 561 nm. Moreover, when DOX was cultured with 4T1 cells for 2 h, red fluorescence appeared, and the red and blue fluorescence overlapped, indicating that DOX could enter into the nucleus. For 4T1 cells incubated with DOX/HMC-Au@PEG, red fluorescence was observed mainly in the cytoplasm, demonstrating that DOX/HMC-Au@PEG was taken up by the cells by endocytosis, and DOX was released into cells. Additionally, to investigate that the effect of NIR irradiation on the DOX release from DOX/HMC-Au@PEG ingested by the cells under NIR irradiation. Cell medium containing DOX/HMC-Au@PEG was poured out and the 4T1 cells were rinsed with PBS. Compared with DOX/HMC-Au@PEG without NIR irradiation, the red fluorescence was stronger under 808 nm laser irradiation, confirming that the release of DOX from DOX/HMC-Au@PEG could be accelerated under NIR irradiation. This could be illustrated by the fact that the increased molecular thermal motion and reduced interactions between HMC and DOX due to the elevated temperature.

The cell viability was evaluated by the MTT assay. Fig. 5(D) and (E) represent the cell viability without/with NIR laser irradiation, respectively. The cell viability of HMC-Au@PEG was higher than 80% without NIR laser irradiation, and the result suggested that the blank carrier had ignorable toxicity and high safety. For the NIR laser irradiation group, the cell viability of HMC-Au@PEG was negatively concentration-dependent, proving that the generated heat that was converted from the NIR laser using HMC-Au@PEG could kill tumor cells. For the free DOX group, whether the NIR laser was irradiated or not, there was a negative correlation between cell viability and DOX concentration. Additionally, there was no significant difference between the two groups, showing that the NIR laser itself did not cause damage to cells. Without NIR laser irradiation, the cell viability of DOX/HMC-Au@PEG was slightly higher than that of the DOX group; however, under 808 nm laser irradiation, the cell viability of DOX/HMC-Au@PEG decreased significantly. This is because the temperature of 4T1 cells increased after the incubation of DOX/HMC-Au@PEG under NIR laser irradiation, and DOX was released faster from DOX/HMC-Au@PEG, which could achieve the synergetic effect. Apart from this, the IC_{50} values for different groups are displayed in Table 2. For the DOX group, no significant difference was found in the IC_{50} values before and after irradiation. However, for the DOX/HMC-Au@PEG group, before and after irradiation, the IC_{50} values declined from 9.675 to 2.713 μg/mL, suggesting that, under NIR laser irradiation, DOX/HMC-Au@PEG could kill tumor cells quickly and HMC-Au could be used as an ideal carrier in tumor treatment. In addition, the CI was used to evaluate the synergistic effect of chemotherapy and PTT: CI < 1 indicates synergism, CI > 1 indicates antagonism, and CI = 1 indicates additive effects. The CI

Table 2
IC_{50} value of HMC-Au@PEG, free DOX and DOX/HMC-Au@PEG groups.

Formulations	IC_{50} (μg/mL)	
	Without NIR irradiation	NIR irradiation
HMC-Au@PEG	–	11.62
free DOX	6.53	6.42
DOX/HMC-Au@PEG	8.97	2.29

value of DOX/HMC-Au@PEG was 0.452 according to Table 2, indicating the synergistic effect of chemotherapy and PTT.

3.5. In vivo combined antitumor therapy and biodistribution study

Thirty female mice were divided into 5 groups—Saline, free DOX, DOX/HMC-Au@PEG, HMC-Au@PEG + NIR and DOX/HMC-Au@PEG + NIR. During the experiment, the body weight and tumor volume of mice were recorded every other day. The changes in the mouse body weight are shown in Fig. 6(A). The weight of mice decreased in the free DOX group; by contrast, it gradually increased in the other 4 groups. This is due to the significant toxicity of free DOX itself; however, the toxicity of DOX could be reduced after DOX is loaded into the carrier. The changes in the tumor volume in mice are shown in Fig. 6(B). For the saline group, the mouse tumor growth was not inhibited and the final tumor volume was approximately 1100 mm^3. In the other 4 groups, the increase in the tumor volume in mice was inhibited to varying degrees. For the DOX/HMC-Au@PEG group, the tumor volume increased from 100 mm^3 to 600 mm^3; in the HMC-Au@PEG + NIR group, the final tumor volume was about 300 mm^3. However, in the DOX/HMC-Au@PEG + NIR group, the final tumor volume was just 145 mm^3, showing the strongest inhibitory effect on tumors. In the 17th day of the experiment, all the mice were killed and the tumor tissue was removed. Fig. 6(C) and (D) show the image of tumor tissue and the weight of the tumor tissue, respectively. Taking the saline group as a comparison, the tumor in DOX/HMC-Au@PEG + NIR group was the smallest and the weight was the lightest. In Fig. 6(E), the images visually showed the changes in temperature in the tumor during irradiation. Under irradiation at 1 W/cm^2 for 3 min, the temperature of the saline group was 37.2 °C; however, for HMC-Au@PEG group, the temperature could reach 46.9 °C under the same irradiation conditions. When the tumor temperature rises above 42 °C and lasts for several minutes, the tumor tissue will be killed. All the results proved that chemo-photothermal synergistic therapy is better for tumor treatment. Additionally, the distribution of DOX at different times was further studied. As exhibited in Fig. 6(F), for free DOX group, DOX was mostly distributed in the tumor at 2 h. Over time, the distribution of DOX in the tumor gradually decreased. This is due to the short half-life of DOX. When DOX was loaded into the HMC-Au@PEG, DOX showed sustained release from the carrier. For the DOX/HMC-Au@PEG group, DOX was mostly distributed in the tumor at 6 h. Moreover, with the gradual clearance of DOX, the accumulation of DOX was decreased in the tumor at 12 h. However, after irradiating the tumor tissue with an 808 nm laser, compared with the group without NIR, the accumulation of DOX was increased obviously and the cumulative amount reached the

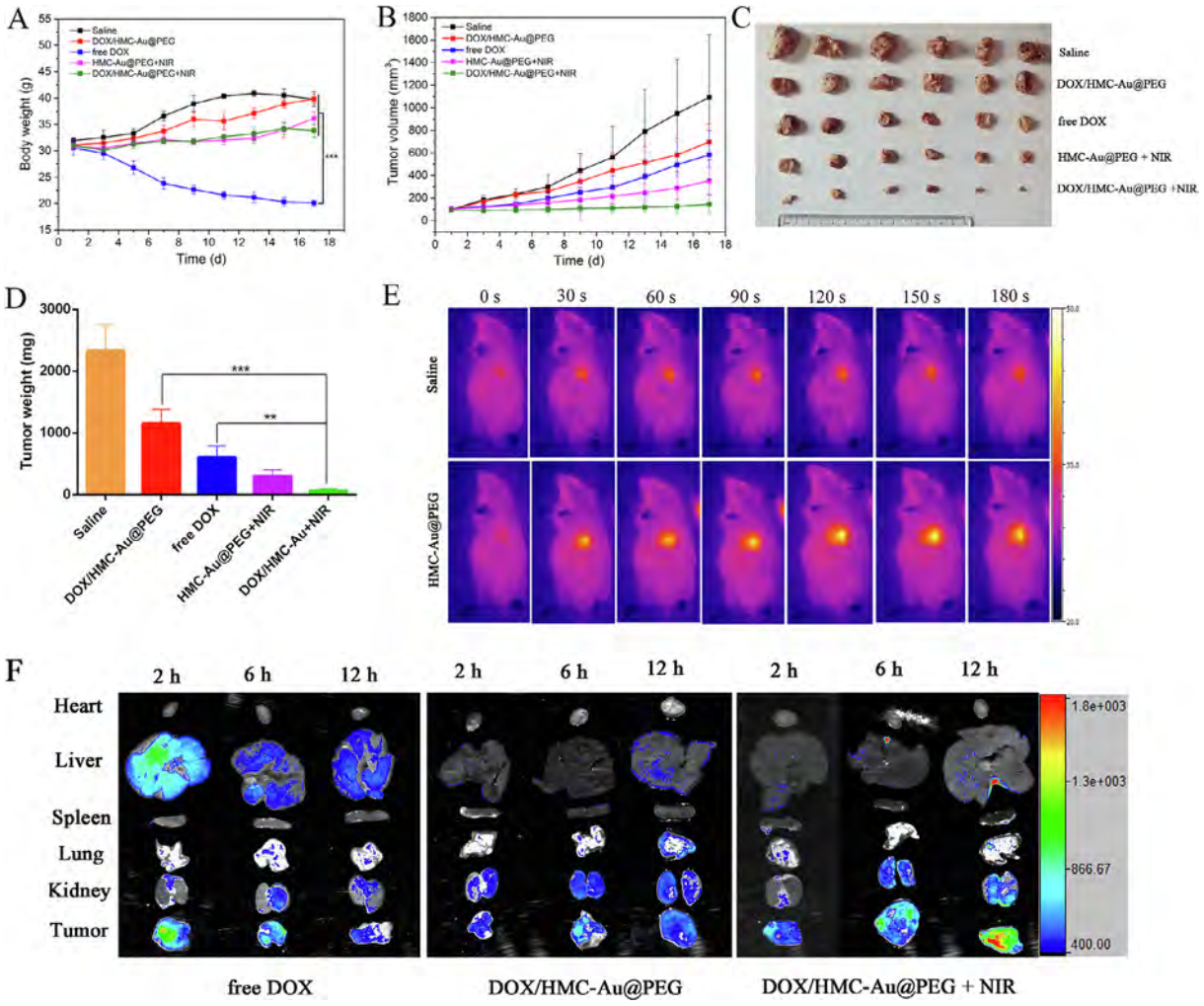

Fig. 6. (A) The body weight of mice (B) tumor volume (C) tumor image (D) tumor weight (E) thermography photographs of mice (** means $p < 0.01$, *** means $p < 0.001$, $n = 6$) (F) Fluorescence photographs of main organs with free DOX and DOX/HMC-Au with or without NIR irradiation at different time points (2 h, 6 h and 12 h, respectively).

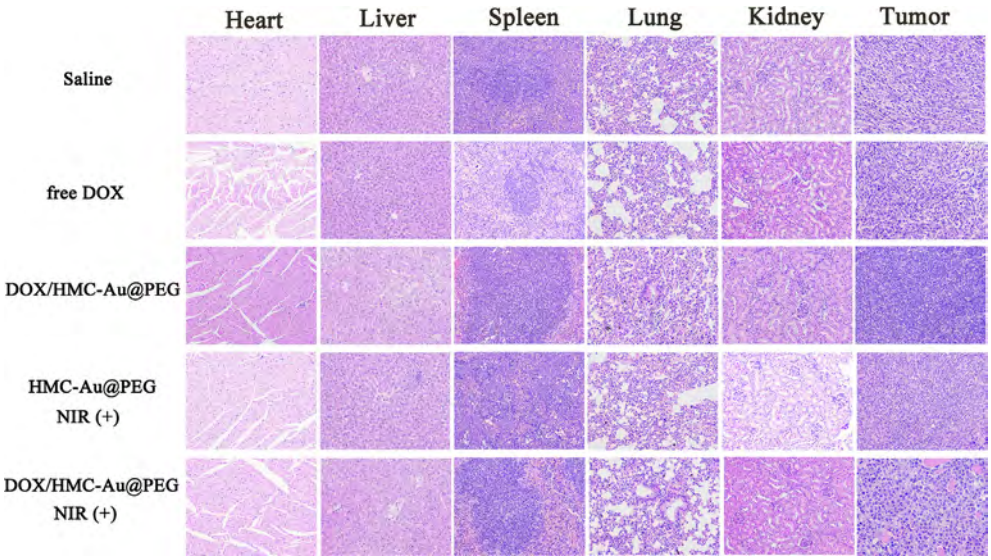

Fig. 7. H&E stained photographs of heart, liver, spleen, lung, kidney and tumor from different groups.

maximum at 12 h. The results suggested that NIR could increase the accumulation of DOX and extend the circulation time of DOX in the tumor.

3.6. Biocompatibility assay

H&E histological analysis was carried out to assess the pathological sections of the tumor, as well as major organs in the mice such as the heart, liver, spleen, lung, and kidney. The results are shown in Fig. 7. For all the groups, no obvious pathological changes were observed in the spleen and lung. However, for the heart of the free DOX group, the muscle gap became wide and myocardial hemorrhage appeared, indicating that the free DOX could cause cardiotoxicity. By contrast, for the DOX/HMC-Au@PEG group and combination therapy group, there was no evident pathological change in the heart, indicating that the nano-carriers can reduce the cardiotoxicity and have good biocompatibility. Additionally, in the tumor tissues, the combination therapy group had the most obvious inhibitory effect. These results suggested that DOX/HMC-Au@PEG could be used as a candidate for cancer treatment.

4. Conclusion

As we all know, both the HMC carrier and gold NPs have a high photothermal conversion efficacy [10,19,28,34]. Therefore, for the first time, HMC and gold NPs were combined to exploit the synergistic effect to increase the photothermal conversion effect of the carrier. In this work, HMC with a large specific surface area and hollow structure was used as a PTT carrier and ensured a high loading capacity of DOX. Additionally, gold NPs could act as gatekeepers to release DOX at the designated location and enhance the photothermal effect of the delivery system. Meanwhile, modification with PEG could enhance the biocompatibility of the system. The final obtained system of DOX/HMC-Au@PEG not only had the redox and NIR dual-responsive properties but also could be used in thermochemotherapy. *In vitro* photothermal experiments indicated that the heating property of the HMC-Au@PEG suspension was more obvious than that of HMC-COOH as well as the mesoporous carbon [32] and gold modified mesoporous silica nanoparticles [28] in the reported literatures. The drug release results suggested that the gold NPs could avoid premature DOX release. Meanwhile, the release of DOX was accelerated under GSH and NIR irradiation. DOX/HMC-Au@PEG had the characteristic of dual-triggered drug release. *In vitro* cytotoxicity assay indicated that DOX/HMC-Au@PEG exhibited a synergistic effect by combinational chemotherapy and PTT. Regarding *in vivo* combined antitumor therapy, the DOX/HMC-Au@PEG + NIR group had the best inhibitory effect on tumors. The current work demonstrated that HMC-Au@PEG can be used as a promising carrier for thermochemotherapy.

Acknowledgements

This work was supported by National Natural Science Foundation of China (No. 81603058 and 81473165), China Postdoctoral Science Foundation (No. 2017M611270), and Career Development Program for Young Teachers in Shenyang Pharmaceutical University (No. ZQN2016025).

Declaration of Competing Interest

We have no conflicts of interest.

Appendix A. Supplementary material

Supplementary data to this article can be found online at https://doi.org/10.1016/j.jcis.2019.07.005.

References

[1] A. Habr-Gama, P.M. de Souza, U. Ribeiro Jr., W. Nadalin, R. Gansl, A.H. Sousa Jr., F.G. Campos, J. Gama-Rodrigues, Dis. Colon Rect. 41 (1998) 1087.
[2] X. Huang, I.H. El-Sayed, W. Qian, M.A. El-Sayed, J. Am. Chem. Soc. 128 (2006) 2115.
[3] J. Kim, S. Park, J.E. Lee, S.M. Jin, J.H. Lee, I.S. Lee, I. Yang, J.S. Kim, S.K. Kim, M.H. Cho, T. Hyeon, Angew. Chem. Int. Ed. 45 (2006) 7754.
[4] K. Yang, L. Hu, X. Ma, S. Ye, L. Cheng, X. Shi, C. Li, Y. Li, Z. Liu, Adv. Mater. 24 (2012) 1868.
[5] L. Cheng, K. Yang, Y. Li, J. Chen, C. Wang, M. Shao, S.T. Lee, Z. Liu, Angew. Chem. Int. Ed. 50 (2011) 7385.
[6] L. Sha, Q. Zhao, D. Wang, X. Li, X. Wang, X. Guan, S. Wang, J. Colloid Interface Sci. 535 (2019) 380.
[7] B. Liu, C. Li, Z. Xie, Z. Hou, Z. Cheng, D. Jin, J. Lin, Dalton T. 45 (2016) 13061.
[8] Y. Li, C. Jiang, D. Zhang, Y. Wang, X. Ren, K. Ai, X. Chen, L. Lu, Acta Biomater. 47 (2017) 124.
[9] Z. Gao, X. Liu, G. Deng, F. Zhou, L. Zhang, Q. Wang, J. Lu, Dalton T. 45 (2016) 13456.

[10] X. Li, X. Wang, L. Sha, D. Wang, W. Shi, Q. Zhao, S. Wang, ACS Appl. Mater. Inter. 10 (2018) 19386.
[11] P.M. Lakhani, S.V. Rompicharla, B. Ghosh, S. Biswas, Nanotechnology 26 (2015) 432001.
[12] S.E. Kim, B.R. Lee, H. Lee, S.D. Jo, H. Kim, Y.Y. Won, J. Lee, Sci. Rep.-UK 7 (2017) 17327.
[13] F. Ratto, P. Matteini, S. Centi, F. Rossi, R. Pini, J. Biophoton. 4 (2011) 64.
[14] X. Wang, C. Wang, L. Cheng, S.T. Lee, Z. Liu, J. Am. Chem. Soc. 134 (2012) 7414.
[15] C. Liang, S. Diao, C. Wang, H. Gong, T. Liu, G. Hong, X. Shi, H. Dai, Z. Liu, Adv. Mater. 26 (2014) 5646.
[16] X. Li, C. Liu, S. Wang, J. Jiao, D. Di, T. Jiang, Q. Zhao, S. Wang, Mat. Sci. Eng. C-Mater. 71 (2017) 594.
[17] J. Bai, Y. Liu, X. Jiang, Biomaterials 35 (2014) 5805.
[18] B. Zhou, Y. Li, G. Niu, M. Lan, Q. Jia, Q. Liang, ACS Appl. Mater. Inter. 8 (2016) 29899.
[19] X. Li, Y. Yan, Y. Lin, J. Jiao, D. Wang, D. Di, Y. Zhang, T. Jiang, Q. Zhao, S. Wang, J. Colloid Interf. Sci. 494 (2017) 159.
[20] M.C. Daniel, D. Astruc, Chem. Rev. 104 (2004) 293.
[21] S. Eustis, M.A. el-Sayed, Chem. Soc. Rev. 35 (2006) 209.
[22] Z. Zhang, J. Wang, C. Chen, Theranostics 3 (2013) 223.
[23] T.T. Järvi, A.C. van Duin, K. Nordlund, J. Phys. Chem. A 115 (2011) 10315.
[24] L.J. Wang, G.M. Rangger, Z.Y. Ma, Q.K. Li, Z. Shuai, E. Zojer, G. Heimel, Phys. Chem. Chem. Phys. 12 (2010) 4287.
[25] G. Saito, J.A. Swanson, K.-D. Lee, Adv. Drug Deliv. Rev. 55 (2003) 199.
[26] C. Wu, H. Guo, J. Hu, Acta Chim. Sinica 67 (2009) 1621.
[27] Q. Zhao, X. Wang, Y. Yan, D. Wang, Y. Zhang, T. Jiang, S. Wang, Eur. J. Pharm. Sci. 99 (2017) 66.
[28] Y. Yang, Y. Lin, D. Di, X. Zhang, D. Wang, Q. Zhao, S. Wang, J. Colloid Interf. Sci. 508 (2017) 323.
[29] J. Wang, J. Rong, Z. Fang, M. Wang, A. Asif, Q. Wu, X. Zhou, X. Ge, Part. Part. Syst. Char. 34 (2017) 1600430.
[30] M.H. Eldakdouki, J. Xia, D.C. Zhu, H. Kavunja, J. Grieshaber, S. O'Reilly, J.J. Mccormick, X. Huang, ACS Appl. Mater. Inter. 6 (2014) 697.
[31] Y. Yang, J. Wan, Y. Niu, Z. Gu, J. Zhang, M. Yu, C. Yu, Chem. Mater. 28 (2016) 9008.
[32] L. Zhou, K. Dong, Z. Chen, J. Ren, X. Qu, Carbon 82 (2015) 479.
[33] H.K. Moon, H.L. Sang, H.C. Choi, ACS Nano 3 (2009) 3707.
[34] A.K. Rengan, A.B. Bukhari, A. Pradhan, R. Malhotra, R. Banerjee, R. Srivastava, A. De, Nano Lett. 15 (2015) 842.